Science of the Total Environment 931 (2024) 172740

Contents lists available at ScienceDirect

Science of the Total Environment

journal homepage: www.elsevier.com/locate/scitotenv

From rust to robust disinfectants: How do iron oxides and inorganic oxidants synergize with UVA light towards bacterial inactivation?

Jialin Jia [a,b,c], Marco Minella [f], Isabel del Castillo González [c], Aurelio Hernández Lehmann [c], Dong Li [d], Nuno P.F. Gonçalves [e,f], Alessandra Bianco Prevot [f], Tao Lin [a,b,*], Stefanos Giannakis [c,**]

[a] Ministry of Education Key Laboratory of Integrated Regulation and Resource Development on Shallow Lakes, Hohai University, Nanjing 210098, PR China
[b] College of Environment, Hohai University, Nanjing 210098, PR China
[c] Universidad Politécnica de Madrid, E.T.S. Ingenieros de Caminos, Canales y Puertos, Departamento de Ingeniería Civil: Hidráulica, Energía y Medio Ambiente, Unidad docente Ingeniería Sanitaria, c/ Profesor Aranguren, s/n, ES-28040 Madrid, Spain
[d] Collaborative Innovation Center of Atmospheric Environment and Equipment Technology, Jiangsu Key Laboratory of Atmospheric Environment Monitoring and Pollution Control, School of Environmental Science and Engineering, Nanjing University of Information Science & Technology, Nanjing 210044, PR China
[e] CICECO – Instituto de Materiais de Aveiro, Departamento de Química, Universidade de Aveiro, Campus Universitário de Santiago, 3810-193 Aveiro, Portugal
[f] Dipartimento di Chimica, Università di Torino, Via Pietro Giuria 5, 10125 Turin, Italy

HIGHLIGHTS

- *E. coli* inactivation in hematite and magnetite-mediated photo-Fenton-like systems was studied.
- PMS can be used as a substitute for H_2O_2 in photo-Fenton process over pH of 5–8.
- HA promoted *E. coli* inactivation in UVA/hematite/PMS and UVA/magnetite/PDS systems.
- ·OH was the main radical in H_2O_2- and PDS-involved photo-Fenton(-like) processes.
- $^1O_2$ was the primary reactive species in PMS-involved photo-Fenton-like processes.

GRAPHICAL ABSTRACT

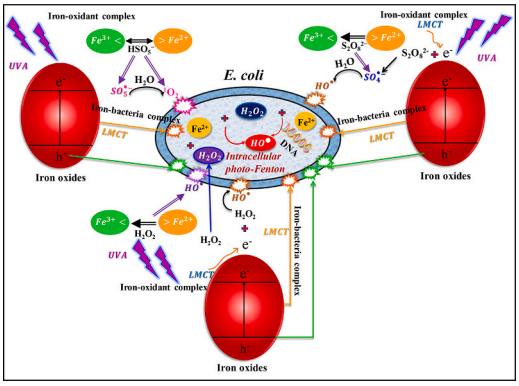

ARTICLE INFO

Editor: Kyle Bibby

Keywords:
Iron oxides
Peroxymonosulfate
Peroxydisulfate

ABSTRACT

Pathogens in drinking water remain a challenge for human health, photo-Fenton process is a promising technique for pathogen inactivation, herein, two common iron oxides, hematite and magnetite mediate persulfate (peroxymonosulfate-PMS - and peroxydisulfate-PDS) involved photo-Fenton-like processes were constructed for *E. coli* inactivation, and the inactivation performance was investigated and compared with the photo-Fenton process under a low intensity UVA irradiation. Results indicated that with a low dose of iron oxides (1 mg/L) and inorganic peroxides (10 mg/L), PMS-involved photo-Fenton-like process is the best substitute for the photo-

* Correspondence to: T. Lin, Ministry of Education Key Laboratory of Integrated Regulation and Resource Development on Shallow Lakes, Hohai University, Nanjing 210098, PR China.
** Corresponding author.
E-mail addresses: 20040076@hhu.edu.cn (T. Lin), stefanos.giannakis@upm.es (S. Giannakis).

https://doi.org/10.1016/j.scitotenv.2024.172740
Received 11 January 2024; Received in revised form 30 March 2024; Accepted 22 April 2024
Available online 26 April 2024

Photo-Fenton
Bacterial inactivation

Fenton one over pH range of 5–8. In addition, humic acid (HA, one of the important components of natural organic matter) incorporated iron oxide-mediated photo-Fenton-like processes for bacteria inactivation was also studied, and facilitating effect was found in UVA/hematite/PMS and UVA/magnetite/PDS systems. Reactive oxygen species (ROS) exploration experiments revealed that ·OH was the predominant radical in H_2O_2- and PDS-containing systems, whereas $^1O_2$ was one of the principal reactive species in the PMS systems. In addition to the semiconductor photocatalysis of iron oxides and UVA-activated oxidants, iron-complexes (iron-oxidant complexes and iron-bacteria complexes) mediated ligand-to-metal charge transfer (LMCT) processes also made contribution to bacterial inactivation. Overall, this study demonstrates that it is feasible to replace H_2O_2 with PMS in a photo-Fenton-like process for water disinfection using a low dose of reagents, mediated by cheap catalysts, such as hematite and magnetite, it is also hoped to provide some insights to practical water treatment.

1. Introduction

The safety of drinking water remains a major global challenge (Brame et al., 2011). Waterborne bacterial pathogens can cause diseases such as cholera, hepatitis A, polio, and diarrhea (Rodríguez-Chueca et al., 2019), which not only pose a threat to public health but also impede economic growth. Although conventional approaches, such as chlorination and ozonation, are effective in removing these pathogens, the potentially risky by-products generated during processing and their inflated costs are drawbacks of these techniques, as well as their limited development in practical applications (Zhou et al., 2022). Therefore, green, safe, economical, and efficient innovative water-disinfection technologies are urgently required.

Advanced oxidation processes (AOPs) have proven to be effective in pathogen inactivation (Meireles et al., 2016; López-Vinent et al., 2021). Iron-based AOPs, such as the photo-Fenton oxidation, have attracted considerable attention as sunlight-assisted oxidative disinfection methods because they can take advantage of visible, near-UV, and UV light, which account for 35 % of the total energy of the solar spectrum (Ruales-Lonfat et al., 2015). Although the stringent pH requirements (acidic condition, pH ~ 2.8) limited the practical application of this technology for contaminant degradation, recent studies have reported that *E. coli* can be effectively inactivated by the photo-Fenton technique at near-neutral pH (Spuhler et al., 2010; Lopez-Vinent et al., 2022; Gualda-Alonso et al., 2023), which provided great possibilities for practical applications.

Among various iron species employed in the photo-Fenton process and their variations, iron oxides are environmentally friendly, low-cost, non-toxic (Xu et al., 2012), and can function as photocatalysts because they often exhibit semiconductor properties (Wu et al., 2022). Many studies have shown that iron oxides can effectively degrade organic pollutants in water (Huang et al., 2001; Andreozzi et al., 2003), but there are limited reports on the use of iron oxides to inactivate bacterial pathogens in photo-Fenton processes (Ruales-Lonfat et al., 2014; Mazille et al., 2010; Asadishad et al., 2013). Ruales-Lonfat et al. investigated the photocatalytic inactivation capacities of four iron oxide (goethite, wüstite, hematite, and magnetite)-mediated photo-Fenton processes at neutral pH, and found that iron oxides can act as both photocatalytic semiconductors and catalysts in the heterogeneous photo-Fenton process applied for bacterial removal (Ruales-Lonfat et al., 2015). However, the oxidation performance of H_2O_2 involved systems is more easily affected by a complex water matrix (e.g., natural organic matter). Moreover, H_2O_2 is not easy to store and transport because of its liquid state and low chemical stability, which limit its practical application. Therefore, there is an urgent need to identify alternative oxidants for AOPs applications.

Recent years, $SO_4^{\bullet-}$-based AOPs that employ peroxymonosulfate (PMS) and peroxydisulfate (PDS) as precursors have attracted considerable attention because of the high redox potential of sulfate radicals (2.6 V vs NHE) and the good chemical stability, and ease of transportation and storage of PMS and PDS (Lopez-Vinent et al., 2022). Moreover, $SO_4^{\bullet-}$ has a stronger selectivity than ·OH towards electron-rich moieties of biomolecules (Buxton et al., 1999), and it has been reported that non-radical pathways often occur in persulfate AOPs, which can greatly avoid the interference caused by water matrices (Wang et al., 2019). $SO_4^{\bullet-}$-based AOPs mediated by PMS and PDS have been successfully used to remove various organic pollutants (Yang et al., 2023; Li et al., 2023a, b). Similar to H_2O_2, they can act as electron acceptors to promote the separation of photogenerated electron-hole pairs in iron oxides, thus improving the oxidation performance of the system. Therefore, PMS and PDS could be considered potentially effective oxidants for use with iron oxides to mediate photo-Fenton-like processes for bacterial inactivation. To date, the effects of $SO_4^{\bullet-}$-based AOPs on pathogen inactivation have not been extensively studied. Moreover, the inactivation mechanism of persulfate-involved photo-Fenton-like systems in bacterial studies remains unclear and requires further investigation.

Therefore, in this study, hematite and magnetite, which are the most common constituents of subsurface environments, were chosen as representative iron oxides for use in PMS- and PDS-based photo-Fenton-like processes. The inactivation performance of different combined systems was evaluated and compared with that of the photo-Fenton process at a neutral pH of 7.5, with a small dose of reagents under UVA irradiation. *Escherichia coli*, a gram-negative bacterium that is the most commonly used indicator of enteric pathogens, was used as a model biological contaminant. Reactive oxygen species (ROS) responsible for bacterial inactivation in each combined system were identified using quenching tests and EPR spectroscopy. In addition, as an important component of natural organic matter (NOM), humic acid (HA) has been found to promote the organic pollutants degradation by iron oxides mediated photo-Fenton-like processes (Gonçalves et al., 2021), while its performance for pathogens inactivation remains unclear, therefore, the HA-incorporated iron oxides that mediate photo-Fenton(-like) processes were also investigated. To the best of our knowledge, this is the first study to investigate the effects of these two iron oxides in PMS- and PDS-involved photo-Fenton-like systems for water disinfection and compare them with those of the traditional photo-Fenton process. The results of this study are expected to provide insights into the practical application of photo-Fenton(−like) processes in water disinfection.

2. Material and methods

2.1. Chemicals

Hydrogen peroxide (H_2O_2, 30 % *w/v*), sodium persulfate (NaS_2O_8), and potassium peroxymonosulfate (Oxone™) were obtained from Merck. Hydrochloric acid (HCl, 36.5 %) and sodium hydroxide (NaOH, 98 %) were purchased from Sigma-Aldrich. Iron chloride ($FeCl_3{\cdot}6H_2O$) and iron sulfate ($FeSO_4{\cdot}7H_2O$) were obtained from Carlo Erba Reagents, whereas HA sodium salts (technical, 50–60 %) from Aldrich-Chemie and ammonium hydroxide (25 %) were obtained from Merck. All solutions were prepared immediately before irradiation with Milli-Q water (18.2 MΩ cm).

2.2. Synthesis of hematite, magnetite, and their HA-containing derivatives

Iron oxides were synthesized using the co-precipitation method under nitrogen atmosphere, as previously reported (Gonçalves et al.,

2020), see the supplementary material for details (TextS1). The physicochemical properties of these two iron oxides are presented in Table 1.

2.3. Characterization of iron oxides

The physicochemical properties of the prepared iron oxides were determined using X-ray diffraction (XRD), scanning electron microscopy (SEM), X-ray photoelectron spectroscopy (XPS), Fourier transform infrared spectroscopy (FTIR), and Brunauer-Emmett-Teller (BET) analysis. In addition, the reactive species in each combined system were detected by electron paramagnetic resonance (EPR) spectroscopy. Additional details are provided in TextS2.

2.4. Bacterial preparation

Escherichia coli K12, a wild-type non-pathogenic strain, was used as the model bacterial strain. The bacteria were stored at −80 °C in cryovials containing 20 % glycerol. To cultivate bacteria, 20 μL of thawed stock was spread onto Plate Count Agar (PCA) and incubated for 24 h at 37 °C. Colonies were spread on a new PCA plate and incubated for another 24 h at 37 °C. The master plate was obtained and stored at 4 °C for approximately two weeks.

Before preparing the bacterial stock, the Luria-Bertani (LB) medium was prepared and sterilized in an autoclave. 5 mL of LB medium was placed in a sterilized flask, and a bacterial colony was taken from the master plate and inoculated into a sterile flask. The flask was incubated overnight at 37 °C, with agitation at 180 rpm. One milliliter of the bacterial stock was collected and centrifuged at 8000 rpm for 2 min, the supernatant was removed, and the pellet was washed twice with sterilized saline solution. The concentration of the final bacterial stock was approximately 10^9 CFU mL^{-1}, which was diluted to 10^6 CFU mL^{-1} for the purpose of the experiment.

2.5. Photocatalytic inactivation experiment

E. coli inactivation experiments were conducted in a 500 mL open beaker containing 150 mL of bacterial suspension. The UVA light was emitted by an array of TLD-type lamps (Philips) with a light intensity of 9.55 ± 0.5 W/m^2. The emission spectrum of the light source is shown in Fig. S1. Before the photocatalytic experiments, the pH of the bacterial suspension was adjusted to 7.5. The inactivation experiments were initiated by introducing a certain amount of iron oxides and oxidants (pre-prepared stocks solution) into the reactor. Throughout the experiment, the temperature in the reactor did not exceed 35 °C. At given time intervals, 100 μL of the solution was withdrawn and quickly spread on a Petri dish or diluted (1:10) with saline solution to ensure measurable colony counts when necessary. The Petri dishes were incubated at 37 °C for 24 h, and the colonies formed were counted manually.

3. Results and discussion

3.1. Characterization of the iron oxides

The morphologies of the synthesized hematite and magnetite were investigated using SEM. As shown in Fig. 1a and b, there is almost no difference in the morphology of the two synthesized iron oxides, which are heterogeneous aggregates composed of particles with dimensions ranging from a few micrometers to tens of micrometers. Both iron oxides exhibited seven characteristic diffraction peaks in the XRD spectrum (Fig. 1c), and the positions of these peaks were almost identical. Based on relevant reports, the locations of the characteristic peaks of hematite and magnetite are close; therefore, some peaks may overlap. However, it can still distinguish some typical peaks of hematite and magnetite; for example, peaks located at 35.6°, 53.9°, and 74.6° could be indexed to the (110), (116), and (622) planes of rhombohedral-phase α-Fe_2O_3 (JCPDS No. 33–0664) (Kolhe et al., 2023), the peaks at 30.1°, 43.4°, 57.5°, and 63.1° could be indexed to the (220), (400), (511), and (440) crystal phases of Fe_3O_4 (JCPDS NO. 19–0629) (Chen et al., 2023). Fig. 1d shows the FT-IR spectra of the two iron oxides. For hematite, the absorption peaks at 577 cm^{-1} and 635 cm^{-1} can mainly be ascribed to the typical stretching vibration of the Fe—O bond (Sundaresan et al., 2023). In addition, the absorption peaks at approximately 1047 cm^{-1} and 1124 cm^{-1} are attributed to the vibration of crystalline Fe—O modes, which can be classified as the characteristic peaks of Fe_2O_3 (Maji et al., 2012; Hao et al., 2015). Compared with hematite, the peaks mentioned above are lower in magnetite, indicating that part of the magnetite may be oxidized to hematite. The broad peak with a maximum at approximately 3403 cm^{-1} was ascribed to the stretching vibration of the surface hydroxyl groups (O—H) of water adsorbed on the surface of the sample (Gaidhane et al., 2023). XPS analyses were also conducted to distinguish between the Fe^{2+} and Fe^{3+} species in the two iron oxides. As shown in Fig. 1e, both iron oxides exhibit two peaks at 710 and 724 eV, which correspond to the Fe 2p3/2 and Fe 2p1/2 signals of Fe^{3+} ions, respectively, indicating the oxidized form of iron on the magnetite surface. It should be noted that although the associated satellite peak at 719 eV is also ascribed to Fe^{3+} species (Emin et al., 2016; Yamashita and Hayes, 2008), the peak intensity of magnetite is much lower than that of hematite, suggesting the presence of Fe^{2+} (Machreki et al., 2024).

Table 1
Physicochemical properties of the studied iron oxides.

Iron oxides	Formula	Iron oxidation state	Isoelectric point (IEP)	Surface area (m^2/g)	Band gap energy (eV)
Hematite	α-Fe_2O_3	+3	8.8	62	1.9
Magnetite	Fe_3O_4	+2, +3	6.6	10	1.45

3.2. E. coli inactivation by the semiconductor photocatalytic action

Firstly, the inactivation performance of iron oxide as photocatalytic semiconductor was evaluated, and it was found that the inactivation performance of hematite was better than that of magnetite under the experimental conditions. In addition, the amount of iron oxides was also optimized, the details are presented in Text S3.

3.3. E. coli inactivation in heterogeneous photo-Fenton-(like) processes

To identify the role of iron oxides in the heterogeneous photo-Fenton-like processes, that is, whether the improvement in inactivation efficiency was attributed to the semiconductor photocatalysis or heterogeneous photo-Fenton-like reactions, inactivation experiments were performed in systems that combined iron oxides with oxidants under UVA irradiation. As shown in the oxidant-only blank experiments in Fig. 2, in the absence of UVA, all three oxidants showed very weak inactivation of *E. coli* within 120 min of reaction time, indicating that under the experimental concentrations, the three oxidants can hardly cause bacterial death. A similar phenomenon was observed in the iron oxide/oxidant systems in the dark, implying that heterogeneous Fenton and Fenton-like processes did not contribute to *E. coli* inactivation (at least at the concentrations used in this study). Previous studies have reported that magnetite can be regarded as a promising Fenton catalyst because it contains +2 and + 3 Fe, which are beneficial for reacting with oxidants to produce reactive species for organic contaminant removal (Matta et al., 2007). However, this was not observed in the present study, possibly because:

(1) At pH 7.5, the magnetite surface is negatively charged, which is not conducive to contact with negatively charged bacteria.

(2) Based on the XPS results (Fig. 1e), most of the surface Fe^{2+} was oxidized to Fe^{3+}, inducing an outer Fe^{3+} oxide layer to form on the surface of magnetite, which would reduce the electron transfer activity

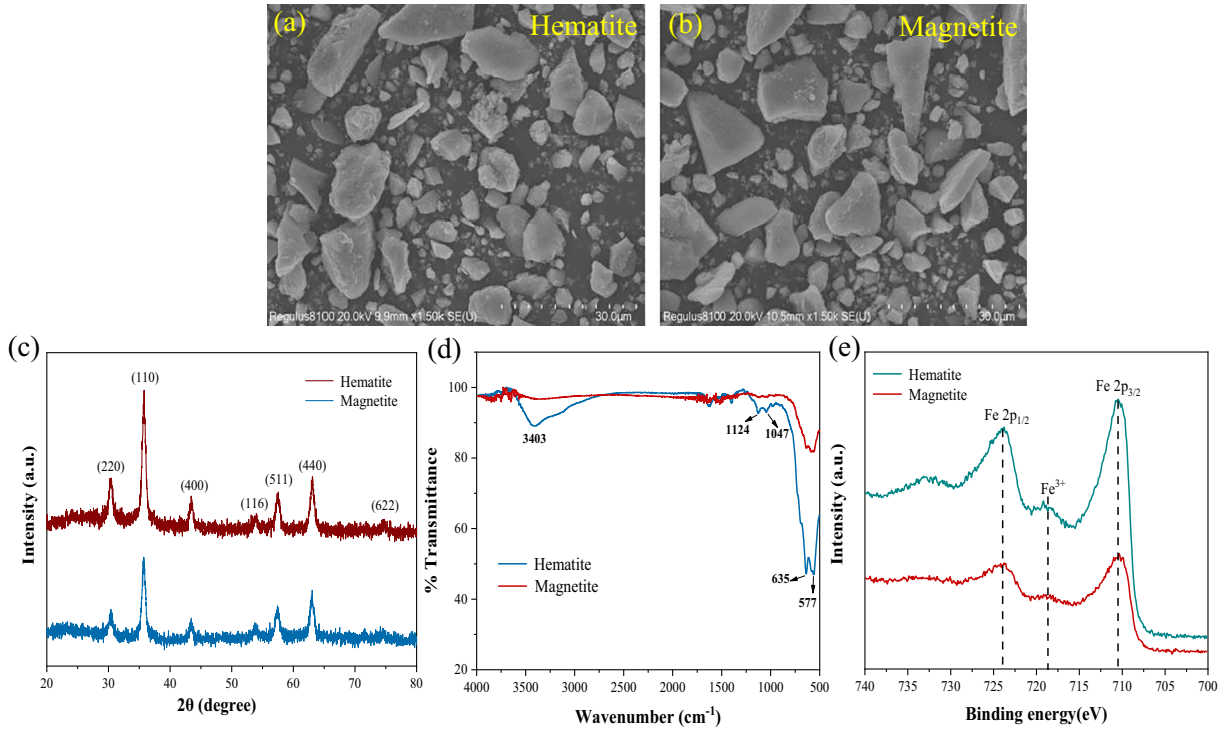

Fig. 1. SEM images of (a) hematite and (b) magnetite; (c) the XRD pattern, (d) FT-IR spectra, and (e) the XPS spectra of Fe 2p of hematite and magnetite.

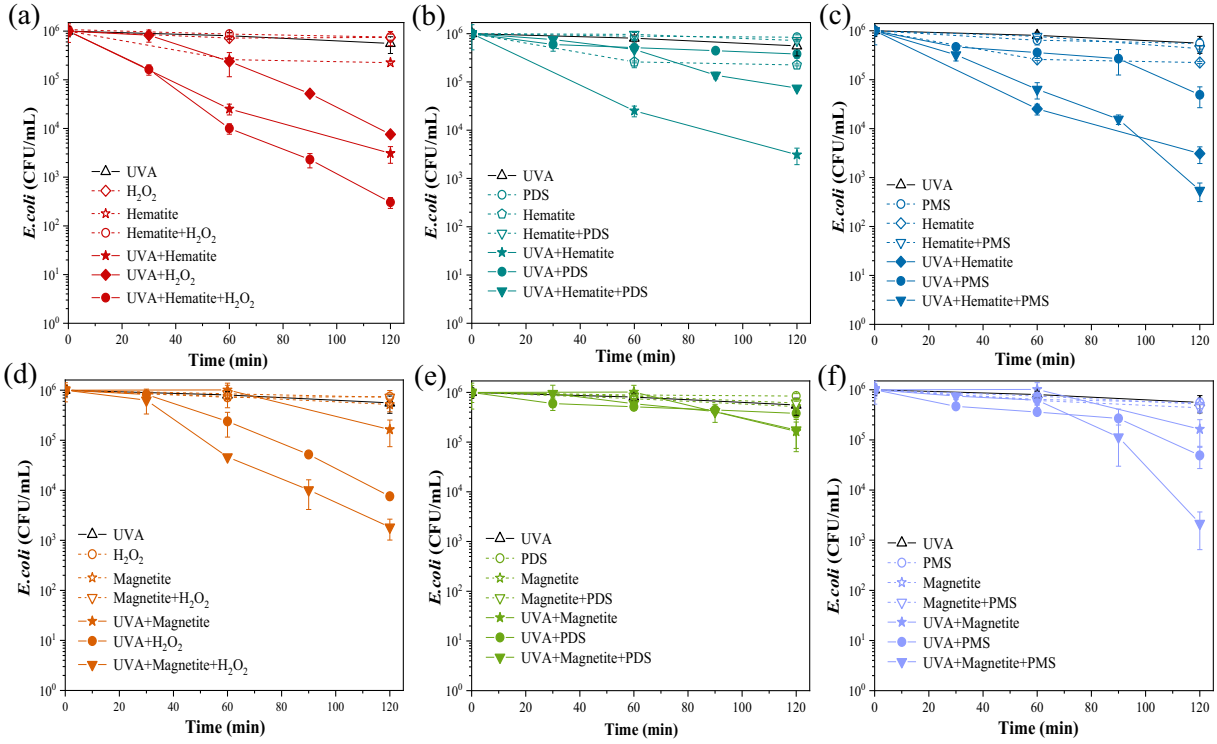

Fig. 2. *E. coli* inactivation by iron oxides in the presence or absence of UVA light and oxidants for (a-c) hematite and (d-f) magnetite. Experimental conditions: [iron oxides] = 1 mg/L, [oxidants] = 10 mg/L, [pH] = 7.5. Experiments were performed in triplicate (the standard error was found to be of ~5 %).

on the surface of magnetite, thus inhibiting the catalytic performance towards Fenton and Fenton-like processes.

(3) Magnetite particles tend to agglomerate because the pH of the reaction system (7.5) is close to the IEP of magnetite (6.6) (Vikesland et al., 2007). Consequently, agglomeration reduces the number of active sites on catalysts, resulting in reduced accessibility to bacteria and oxidants.

When the three oxidants were subjected to UVA irradiation, the inactivation outcomes followed the sequence: UVA + H_2O_2 > UVA + PMS > UVA + PDS. With H_2O_2, approximately 2-logU bacterial

inactivation was achieved within 120 min, which was higher than that with PMS (approximately 1.4 logU) and PDS (approximately 0.4 logU). This could be attributed to the fact that H_2O_2 can be transported into the cells of bacteria; although it is normally scavenged by enzymes with antioxidant action, these enzymes can be inactivated under UVA (even partially) and the intracellular Fenton reaction can initiate (Eqs. (1) and (2)). Hence, H_2O_2 penetration and UVA exposure weaken the defenses of bacteria, leading to higher inactivation.

$$\text{Intracellular Fenton reaction}: Fe^{2+} + H_2O_2 \rightarrow Fe^{3+} + \cdot OH + OH^- \quad (1)$$

$$\text{Intracellular } Fe^{3+} \text{ photo} - \text{reduction}: Fe(OH)^{2+} + h\nu \rightarrow Fe^{2+} + \cdot OH \quad (2)$$

PMS is able to mono-electronically oxidize the bacterial cell wall, which acts as an electron donor, producing both ·OH and $SO_4^{\bullet-}$ (Eqs. (3) and (4)) (Tian et al., 2024). For PDS, an analogous reaction produced only $SO_4^{\bullet-}$ (Eq. (5)) (Lopez-Vinent et al., 2022). Based on previous reports, the reactivity of ·OH with biomolecules is ten times higher than that of $SO_4^{\bullet-}$ (Rodríguez-Chueca et al., 2019; Anipsitakis et al., 2008). Thus, considering the intracellular action of H_2O_2 and the predominant extracellular oxidation of PMS/PDS, clear differences among the three oxidants were observed.

$$HSO_5^- + e^- \rightarrow SO_4^{\bullet-} + OH^- \quad (3)$$

$$HSO_5^- + e^- \rightarrow SO_4^{2-} + \cdot OH \quad (4)$$

$$S_2O_8^{2-} + e^- \rightarrow SO_4^{2-} + SO_4^{\bullet-} \quad (5)$$

When the three factors were combined (iron oxides/oxidants/UVA), except for the PDS-containing systems, *E. coli* inactivation was significantly enhanced compared to their constituent systems (Fig. 2a-e). This is due to:

(1) Heterogeneous activation. The system shifts from dominant semiconductor photocatalytic inactivation mediated by iron oxides to heterogeneous activation of peroxides (Eqs. (6)–(11)) (Lopez-Vinent et al., 2022). (≡ indicates a reaction at the surface of the oxides)

$$HSO_5^- + \equiv Fe^{3+} \rightarrow \equiv Fe^{2+} + SO_5^{\bullet-} + H^+ \quad (6)$$

$$HSO_5^- + \equiv Fe^{2+} \rightarrow \equiv Fe^{3+} + SO_4^{\bullet-} + OH^- \quad (7)$$

$$H_2O_2 + \equiv Fe^{2+} \rightarrow \equiv Fe^{3+} + OH^- + \cdot OH \quad (8)$$

$$H_2O_2 + \equiv Fe^{3+} \rightarrow \equiv Fe^{2+} + HO_2^{\bullet} + H^+ \quad (9)$$

$$S_2O_8^{2-} + \equiv Fe^{2+} \rightarrow \equiv Fe^{3+} + SO_4^{\bullet-} + SO_4^{2-} \quad (10)$$

$$S_2O_8^{2-} + \equiv Fe^{3+} + 1/2\ O_2 \rightarrow SO_4^{\bullet-} + \equiv Fe^{2+} + SO_4^{2-} + FeO^{2+} \quad (11)$$

Leaching is another factor that could occur when solid catalysts are involved in the reaction. Potential Fe leaching from the surfaces of oxides may lead to a homogeneous activation reaction (Jiménez et al., 2020). However, in the explored experimental conditions it was not detected dissolved Fe; increasing the concentration of iron oxides to 100 mg/L at pH = 3, 0.1 mg/L total Fe was leached from hematite (data not shown). Hence, possible participation in homogeneous reactions can be safely discarded.

(2) Oxidants: When oxidants were added to a system, the semiconductor mode was no longer the only inactivation pathway. Under light excitation, iron oxides produce photogenerated electrons and holes in the valence band (h_{VB}^+) and conduction band (e_{CB}^-), respectively (Eqs. (12) and (13)). As good electron acceptors, peroxides can react with e_{CB}^- to generate radicals (Eqs. (14)–(16)). This not only increases the radical concentration in the reaction system but also improves the separation of the photogenerated electron-hole pairs, leading to higher inactivation efficiency. The inactivation efficiency of the hematite-mediated combined system was higher than that of magnetite, which could be attributed to the inherent photocatalytic features of the two oxides.

$$Fe_2O_3 + h\nu \rightarrow Fe_2O_3\ (e_{CB}^- + h_{VB}^+) \quad (12)$$

$$Fe_3O_4 + h\nu \rightarrow Fe_3O_4\ (e_{CB}^- + h_{VB}^+) \quad (13)$$

$$e_{CB}^- + H_2O_2 \rightarrow OH^- + \cdot OH \quad (14)$$

$$e_{CB}^- + S_2O_8^{2-} \rightarrow SO_4^{\bullet-} + SO_4^{2-} \quad (15)$$

$$e_{CB}^- + HSO_5^- \rightarrow SO_4^{\bullet-} + \cdot OH \quad (16)$$

Furthermore, in addition to the direct attack of h_{VB}^+ on bacteria with consequent inactivation, h_{VB}^+-mediated activation of oxidants is known to generate reactive species that may contribute to bacterial inactivation, namely PMS radicals and singlet oxygen ($^1O_2$) (Eqs. (17)–(20)) (Ruales-Lonfat et al., 2015; Machreki et al., 2024).

$$HSO_5^- + h_{VB}^+ \rightarrow SO_5^{\bullet-} + H^+ \quad (17)$$

$$2SO_5^{\bullet-} + H_2O \rightarrow 2HSO_5^- + {}^1O_2 \quad (18)$$

$$H_2O_2 + h_{VB}^+ \rightarrow O_2^{\bullet-} + 2H^+ \quad (19)$$

$$h_{VB}^+ + O_2^{\bullet-} \rightarrow {}^1O_2 \quad (20)$$

(3) Bulk ligand-to-metal charge transfer: Under neutral pH conditions, Fe ions are barely soluble in water. However, iron-oxidant complexes are formed on the surface of suspended iron oxides. Under light irradiation, the formed complexes can be photochemically activated by the generation of reactive species via ligand-to-metal charge transfer (LMCT) mechanism (Hasan et al., 2020).

(4) Cell envelope ligand-to-metal charge transfer: Iron oxides can also form complexes with the components of bacterial cell walls, with the latter being an electron donor (Ruales-Lonfat et al., 2014). Under light irradiation, an effective LMCT process can damage the bacterial integrity (Eq. (21)). Simultaneously, the generated Fe^{2+} would, in turn, enhance intracellular Fe^{2+} diffusion to promote the photo-Fenton process (Spuhler et al., 2010; García-Fernández et al., 2012).

$$[Fe(COO-R)]^{2+} + h\nu \rightarrow Fe^{2+} + CO_2 + R^{\cdot} \quad (21)$$

Although there were no extraordinary differences in the inactivation efficiencies of the UVA/hematite/H_2O_2 ($k = 0.068 \pm 0.0034\ min^{-1}$) and UVA/hematite/PMS systems ($k = 0.06\ min^{-1} \pm 0.0077\ min^{-1}$), as well as UVA/magnetite/H_2O_2 ($k = 0.056 \pm 0.0056\ min^{-1}$) and UVA/magnetite/PMS ($k = 0.051\ min^{-1} \pm 0.016\ min^{-1}$) systems (Table S1), the synergistic factors (based on Eq. (22)) of the different systems followed the order: $S_{hematite/H2O2/UVA} = 6.18 > S_{magnetite/H2O2/UVA} = 4.44 > S_{hematite/PMS/UVA} = 4.41 > S_{magnetite/PMS/UVA} = 3.4 > S_{hematite/PDS/UVA} = 2.3 > S_{magnetite/PDS/UVA} = 1.22$. Except for the H_2O_2-involved systems, the PMS-involved systems have higher synergy effects than PDS systems, and the synergy factors of hematite- and magnetite-mediated PMS systems were 2.06 and 2.69 times higher than those of PDS systems, indicating that PMS might be considered as a good alternative oxidant to be employed in the photo-Fenton-like process.

$$S_{iron\ oxides/oxidants/UVA} = \frac{k_{iron\ oxides/oxidants/UVA}}{k_{iron\ oxides} + k_{oxidants} + k_{UVA}} \quad (22)$$

The introduction of PDS did not improve the inactivation performance (Fig. 2b and e) of the hematite-mediated system, in which the inactivation efficiency of the system decreased with the addition of PDS. Previous studies have reported that compared to PMS, PDS is not easily activated by Fe, Zn, etc., and its activation efficiency is lower than that of PMS (Li et al., 2023a, b). Notably, the Fe^{3+} reduction by PDS (Eq. (11)) is an extremely slow process that leads to low inactivation performance.

For hematite, the added oxidants did not significantly improve the inactivation performance of the photocatalytic system, with the k_{obs}

values of the UVA/hematite/H_2O_2 and UVA/hematite/PMS systems being only 1.4 and 1.3 times higher than that of the UVA/hematite system. The introduction of PDS also did not significantly improve the inactivation performance of UVA/magnetite system ($S_{magnetite/PDS/UVA}$ = 1.2), however, when H_2O_2 and PMS were added to the UVA/magnetite system, an enhanced inactivation was observed, with the k_{obs} of UVA/magnetite/H_2O_2 and UVA/magnetite/PMS systems 4.7 and 4.3 times higher than that of the UVA/magnetite system. Thus, based on the above analysis, it can be concluded that a low concentration of hematite (1 mg/L) alone can be used as a semiconductor photocatalyst to inactivate bacteria without the addition of oxidants. This is meaningful because the omission of oxidants can significantly decrease treatment costs. As a provisional conclusion, we suggest that since PDS did not play a positive role in the investigated photo-Fenton-like system, whereas PMS enhanced the inactivation performance of the UVA/magnetite system, the above results are expected to provide a reference for oxidants chosen in practical scenarios.

3.4. Effect of pH on the inactivation performance of photo-Fenton(-like) systems

The inactivation efficiencies and corresponding reaction kinetic constants of the different combined systems over a wide pH range are shown in Fig. 3. At pH 5, both the inactivation efficiencies and kinetic rates (Fig. S4) of the magnetite-containing systems were higher than those of the hematite systems. As mentioned previously, the IEP of magnetite is 6.6; therefore, the surface of magnetite at pH 5 is positively charged, whereas the bacterial membrane is negatively charged. Owing to electrostatic attraction, more bacteria are attached to the magnetite surface, and the adsorption of microorganisms onto magnetite is a prerequisite for attaining significant inactivation (Nieto-Juarez and Kohn, 2013). In addition, over a wide pH range, PMS exists in the form of anions (Elias et al., 1994) (pK_{a1} = 0.4 and pK_{a2} = 9.3); thus, the probability of interaction between magnetite and PMS increases. It has been reported that the reaction rate of PMS and Fe^{2+} of magnetite is the highest (k = 3.0 × 10^4 M^{-1} s^{-1}) among Fe^{2+}/Fe^{3+} with the three investigated oxidants (Lopez-Vinent et al., 2022), resulting in the highest bacterial inactivation among the six systems.

As the pH increased, the inactivation efficiency of the hematite-mediated system increased. In addition to the PMS-involved system, the inactivation efficiencies of the magnetite-mediated PDS and H_2O_2 systems were lower than those of the hematite-mediated systems. At pH values of 6 and 7, significant agglomeration of magnetite with a consequent decrease in the surface area may occur because of the IEP of magnetite (6.6). Additionally, the magnetite surface was negatively charged at pH 8, leading to a more difficult adsorption process for *E. coli* and the interaction of the oxidants with the magnetite surface. However, the inactivation efficiency of hematite-mediated systems gradually decreases as the pH value increases, which could be because the positive charge on the hematite surface gradually decreases, resulting in less opportunity for oxidants and bacteria to be adsorbed, thereby reducing inactivation efficiency.

In conclusion, the *E. coli* inactivation performance of the UVA/hematite/H_2O_2 system was not affected (total inactivation was achieved within 180 min) by changes of pH 5–7. The PMS-involved system could achieve totally inactivation in pH of 5–7, but with the inactivation

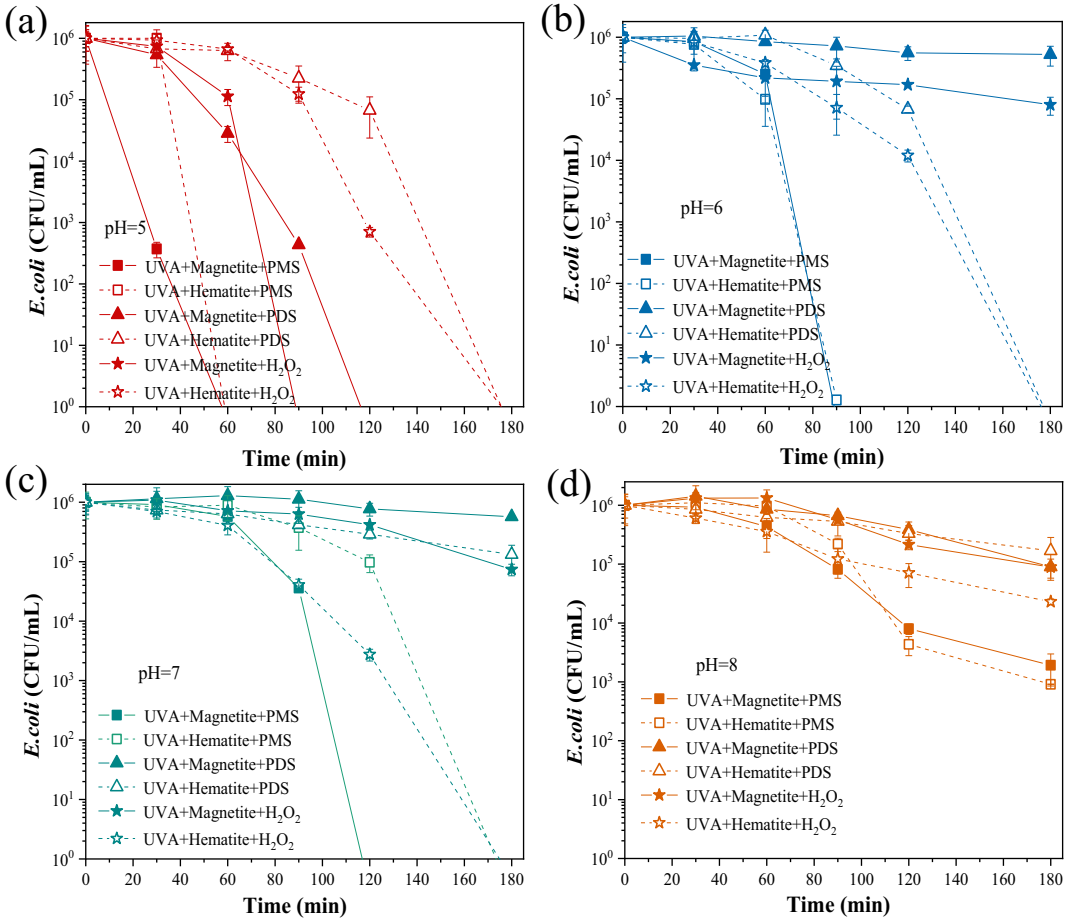

Fig. 3. *E. coli* inactivation in UVA/iron oxide/oxidant systems at pH values of (a) 5, (b) 6, (c) 7, (d) 8, and (e) corresponding kinetic rates. Experimental conditions: [iron oxides] = 1 mg/L, [oxidants] = 10 mg/L, [pH] = 7.5. Experiments were performed in triplicate (the standard error was found to be of ~5 %).

performance decreased with pH increased (the total inactivation time gradually increased). The UVA/magnetite/H_2O_2 and the PDS-containing system exhibited the best bacteria inactivation only at pH 5, while showed poor inactivation at pH 6–8.

3.5. The inactivation performance of humic acid incorporated iron oxide mediated photo-Fenton(-like) processes

Humic acid (HA) is widely distributed in water bodies and sediment. Owing to its complex structure and composition, its adsorption, redox, and complexation characteristics have potential effects on the migration and transformation of environmental pollutants (Zhang et al., 2020). It has been reported that HA can complex soluble iron and iron oxides through different functional groups, such as phenolic, carboxylic, and carbonyl groups (Niu et al., 2011), and promote (Rose and Waite, 2003) or inhibit (Colón et al., 2008) the degradation of organic pollutants. In previous studies, HA-coated magnetite particles have been found to be highly efficient heterogeneous photo-Fenton materials for organic pollutant removal (Gonçalves et al., 2020; Gonçalves et al., 2021). However, the photo-Fenton(−like) process mediated by HA-modified iron oxides for pathogens inactivation remains unclear. For this reason, the *E. coli* inactivation in HA-coated hematite and magnetite-mediated photo-Fenton(−like) processes were explored.

First, the role of HA in iron oxide semiconductor photocatalysis processes was evaluated. As shown in Fig. S5, with the incorporation of different amounts of HA, the inactivation performance of both iron oxide-mediated systems showed an inhibitory trend, indicating that HA did not produce a positive effect on *E. coli* inactivation. It has been reported that the photoreduction of Fe^{3+}-complexes can give Fe^{2+} and ligand radicals (Eq. (23)), which can react with O_2 to generate reactive species (Pignatello et al., 2006).

$$Fe^{3+}—(L)_n + h\nu \rightarrow Fe^{2+}—(L)_{n-1} + L^{+}ox^{\bullet} \quad (23)$$

However, this was not the case in the present study, and there was no significant difference in inactivation performance between samples with 0.5 % and 4 % HA. This may be because, although more HA might induce more Fe-organo-complex formation, the negative effects of HA (such as the quenching of reactive species and the shielding of UVA light towards iron oxide) were presumably greater than the positive effect.

When oxidants were introduced into hematite-mediated system, the inactivation performance of both H_2O_2- and PDS-containing systems was delayed, and the inhibition in PDS system was lower than that of H_2O_2 system (Fig. 4a and b). Similar to the photocatalytic processes, there were no significant differences in the inactivation performance between the samples with 0.5 % and 4 % HA, which could be ascribed to the same reason, as previously discussed. However, when PMS was added into the system, the inactivation performance of both 0.5 % and 4 % HA groups was remarkably improved; with 6 logU inactivation achieved within 90 min (Fig. 4c). The kinetic constants of different systems were shown in Fig. S6. As discussed in Section 3.7 (vide infra), $^1O_2$ is the predominant reactive species in UVA/hematite/PMS system, so the radical quenching effects brought by HA was avoid. The deactivation in the first 60 min could be attributed to the light-shielding effect caused by HA, which makes the generation of $^1O_2$ ineffective in the system. As the reaction proceeds, Eq. (23) occurred and begin to dominate the reaction system. The reaction constant of Fe^{2+} with PMS is 3.0×10^4 M^{-1} s^{-1}, which has been reported to have the highest value among Fe^{2+}/Fe^{3+} with H_2O_2, PDS, and PMS (Lopez-Vinent et al., 2022), thus achieving higher inactivation efficiency. Moreover, the excess HA might also be excited by light and then activate PMS to generate a series of reactive species, such as $SO_4^{\bullet-}$, ·OH, and $^1O_2$, where $^1O_2$ played a dominant role in the system (Jia et al., 2020). Because of the longer lifetime (3–5 μs) of $^1O_2$ and the absence of antioxidant enzymes in bacterial cells (Giannakis et al., 2021), $^1O_2$ is more selective and sensitive to bacterial moieties such as proteins, lipids, and nucleic acids (Walling and Goosen, 1973), thus leading to an enhanced inactivation efficiency of the UVA/hematite/PMS system.

When H_2O_2 was added to the magnetite system, the inactivation efficiency of 0.5 % HA group was severely inhibited (Fig. 4d), with a kinetic constant was approximately 5.1 times (k = 0.011 ± 0.0021

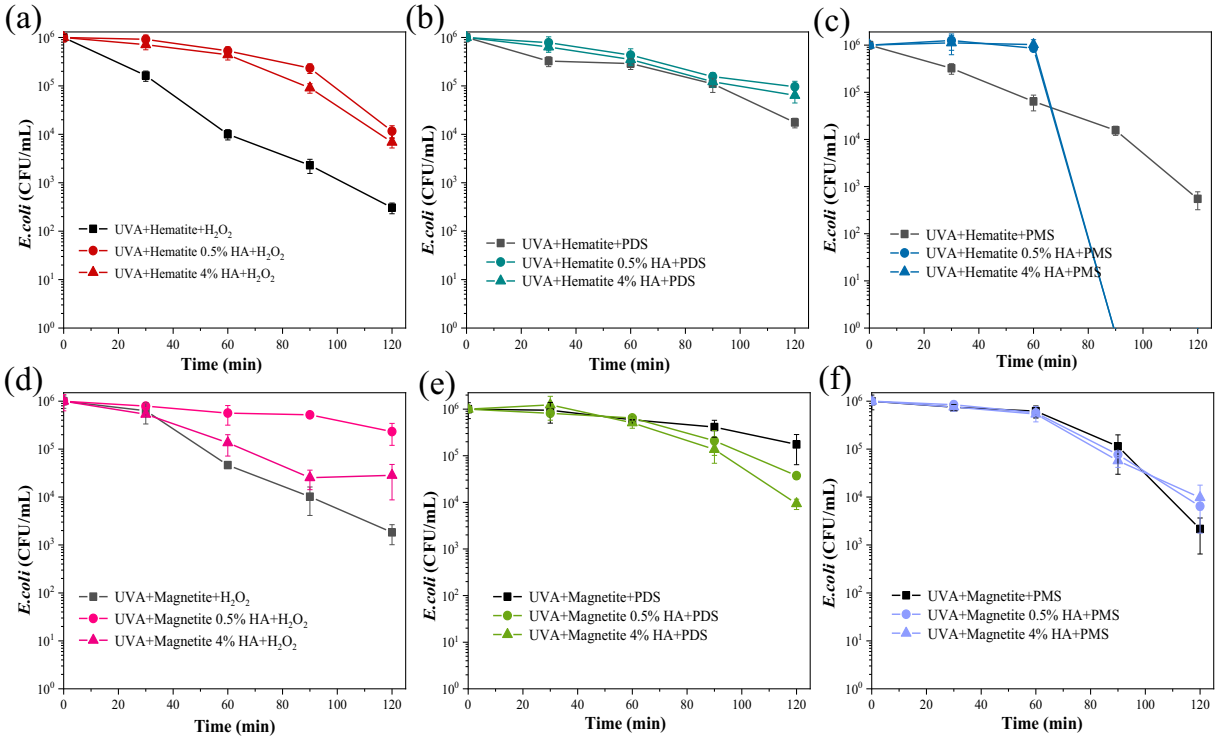

Fig. 4. *E. coli* inactivation in the UVA/HA/iron oxide/oxidant systems. Experimental conditions: [iron oxide] = [iron oxide/HA] = 1 mg/L, [oxidant] = 10 mg/L, [pH] = 7.5. Experiments were performed in triplicate (the standard error was found to be of ~5 %).

min^{-1}) lower than that of the UVA/Magnetite/H_2O_2 system (k = 0.056 ± 0.0056 min^{-1}) (Fig. S6). With the addition of HA increased to 4 %, the degree of inhibition decreased (k = 0.034 ± 0.0054 min^{-1}, 1.6 times lower than that of the UVA/Magnetite/H_2O_2 system). It has been reported that the carboxylic moieties of HA are effective ligands for Fe^{+2} and Fe^{+3}, the formed iron-complexes are not only redox-active species that can react with oxidants but also photoactive species (Gonçalves et al., 2021). Hence, in addition to the negative effects brought by HA mentioned earlier, it can be reasonable hypothesized that the reaction rate of the formed Fe-complex with H_2O_2 being lower than that of Fe^{2+}-H_2O_2 (k = 63–76 M^{-1} s^{-1}), and the positive effect (e.g. photoactive species) exert by 0.5 % HA system is small. As the amount of HA increased (4%HA), the positive effect induced by the iron-complex would offset a part of negative effect, so the inhibition was reduced. For PDS system, the inactivation efficiency improved with the increment of HA load (Fig. 4e), which might be due to that the reaction constant of iron-complex with PDS was higher than that of Fe^{2+}-PDS (k = 12–27 M^{-1} s^{-1}) as well as the positive effects of the photoactive of iron-complex, and the positive effects was greater than the negative effect in the system. As for PMS system, the inactivation performance was slightly retarded in both 0.5 % HA and 4 % HA systems, and the degree of inhibition was similar in both systems. As discussed in Section 3.7, $^1O_2$ is also the main reactive species in the UVA/magnetite/PMS system; therefore, the radical quenching effect caused by HA did not occur. In addition, magnetite was negatively charged under these experimental pH conditions, and HA was negatively charged at this pH. Therefore, compared with the hematite group, fewer Fe-organo-complexes were formed owing to the electrostatic repulsion effect, resulting in less generated Fe^{2+} reacting with PMS to produce reactive species compared to hematite systems. The slight inhibitory effect could be considered as the result of positive and negative effects of HA in the system.

The interaction mechanism between iron, HA, and oxidants is complicated, the above data can only partially clarify it. Although previous studies have reported that the addition of humic(−like) substances significantly enhanced organic pollutant removal in Fenton or photo-Fenton processes, the positive role of humic(−like) substances in the oxidation mechanism of above processes have not been fully elucidated, owing to the complex structure and composition of HA as well as its complex reactions with iron and oxidants (Carlos et al., 2012; García-Ballesteros et al., 2018; Aparicio et al., 2019; Gonçalves et al., 2021). Given that HA are widely distributed in nature, and iron oxides are cheap and effective iron sources in photo-Fenton-like processes, the interaction mechanism between iron, HA, and oxidants deserves further exploration in the future.

In addition, considering the probable different application scenarios in practical application, the high-dose iron oxide(-HA) and oxidant-involved photo-Fenton-like systems for *E. coli* inactivation were also investigated; and the details were presented in TextS4.

3.6. Identification of reactive oxygen species in photo-Fenton-like systems

3.6.1. EPR experiments

EPR characterization was conducted to explore the reactive species in each combined system. For the H_2O_2-involved system, based on previous studies (Feng and Zhang, 2023; Pino-Sandoval et al., 2023), it can be safely assumed that ·OH played a dominant role. The reactive species formed in the persulfate-containing systems were evaluated using EPR spectroscopy. As shown in Fig. 5, when 5, 5-dimethyl-1-pyrroline (DMPO) was employed as a spin-trapping reagent for $SO_4^{\bullet-}$ and ·OH, the characteristic signals of the DMPO-SO_4 and DMPO-OH adducts

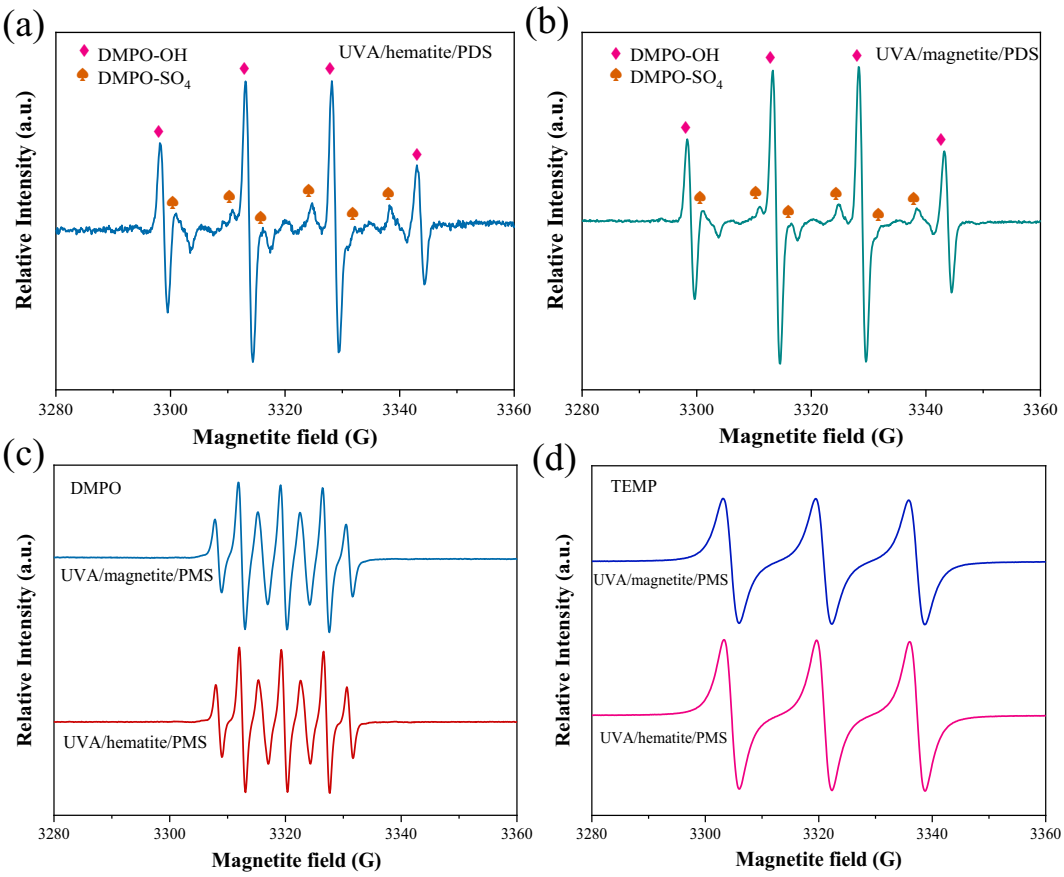

Fig. 5. Reactive species analysis in different photo-Fenton-like systems. EPR tests of ·OH and $SO_4^{\bullet-}$ in (a) UVA/hematite/PDS system, (b) UVA/magnetite/PDS system, and (c) PMS involved systems; (d) EPR tests of $^1O_2$ in PMS involved systems. Experimental conditions: [iron oxide] = 1 mg/L, [oxidants] = 10 mg/L, [pH] = 7.5.

appeared in both the UVA/hematite/PDS and UVA/magnetite/PDS systems, where ·OH mainly originated from the oxidation of water by $SO_4^{\bullet-}$ (Eq. (24)).

$$SO_4^{\bullet-} + H_2O \rightarrow SO_4^{2-} + \cdot OH + H^+ \quad (24)$$

However, no characteristic peaks of the DMPO-SO_4 and DMPO-OH adducts were observed in the PMS system, and characteristic peaks of the DMPOX adducts appeared in both the UVA/hematite/PMS and UVA/magnetite/PMS systems (Fig. 5c). Previous studies have reported that the oxidized derivative (DMPOX) can be formed by the reaction between the carbon surface-bound oxidative complexes/$^1O_2$ and DMPO (Jiang et al., 2018; Li et al., 2018). The formation of DMPOX has also been documented with PMS under both solar irradiation and in the dark but in the presence of chloride (Berruti et al., 2023). In the present study, $^1O_2$ was the most likely source of DMPOX. To confirm this, EPR experiments employing TEMP as a spin-trapping reagent for $^1O_2$ were conducted to provide further evidence. As shown in Fig. 5d, a noticeable 1:1:1 triplet signal corresponding to TEMP-$^1O_2$ adducts (TEMPO) appears in both the UVA/hematite/PMS and UVA/magnetite/PMS systems, indicating the presence of $^1O_2$ in the PMS systems.

3.6.2. Quenching experiments

Quenching experiments were performed using selective radical scavengers to investigate the reactive species further involved. Isopropanol (IPA) has been reported as a trapping agent for both ·OH and $SO_4^{\bullet-}$ ($k_{\cdot OH,\ IPA} = 1.9 \times 10^9\ M^{-1}\ s^{-1}$, $k_{SO_4^{\bullet-},IPA} = 8.6 \times 10^7\ M^{-1}\ s^{-1}$), whereas *t*-butanol (TBA) is more selective for quenching ·OH ($k_{\cdot OH,\ TBA} = 3.1 \times 10^9\ M^{-1}\ s^{-1}$) than $SO_4^{\bullet-}$ ($k_{SO_4^{\bullet-},TBA} = 8.4 \times 10^5\ M^{-1}\ s^{-1}$) (Jia et al., 2020). When TBA was added to the H_2O_2 system, the inactivation efficiency was seriously inhibited, and as the concentration of TBA increased to 0.5 mM, the inactivation was almost completely blocked (Fig. 6a and d), confirming that ·OH was the main radical responsible for bacterial inactivation in H_2O_2-contained systems.

When IPA and TBA were added separately to the PDS-containing systems, the inactivation efficiencies of the UVA/hematite/PDS and UVA/magnetite/PDS systems were significantly inhibited. For the UVA/hematite/PDS system, the degree of inhibition was enhanced with the increment of their concentration, and the inactivation was completely inhibited at the concentration of 0.5 mM of the two scavengers. In the case of the UVA/magnetite/PDS system, the inactivation performance could be inhibited even with 0.1 mM scavengers, which could be due to the fewer radicals generated in the system because the inactivation efficiency was lower than that of the UVA/hematite/PDS system. Notably, IPA and TBA are toxic to bacteria beyond a certain level. However, when the concentration of the two scavengers was increased from 0.1 to 0.5 mM, *E. coli* inactivation showed a decreasing trend, indicating that the employed concentrations did not cause bacterial death. Combined with the EPR results, it can be concluded that both $SO_4^{\bullet-}$ and ·OH are responsible for *E. coli* inactivation in the PDS-involved systems, and ·OH plays a dominant role.

The inactivation performance of the PMS-involved system was severely suppressed when IPA was added to it. Surprisingly, when TBA was introduced into the system, the inactivation efficiency of both systems dramatically improved (Fig. 6c and f). EPR results have revealed that $^1O_2$ was present in the PMS-involved systems, to further confirm this result, inactivation experiments were conducted in D_2O, since $^1O_2$ lives more than 10 times longer in D_2O (20–30 μs) than in H_2O (2 ms) (Dong et al., 2021). Fig. S9 reveals that the inactivation efficiency of the PMS-involved system in D_2O was higher than that in H_2O, indicating the presence of $^1O_2$ in the PMS system. The phenomenon after adding IPA and TBA might be ascribed to the fact that PMS could directly oxidize IPA and thus be consumed, leading to less formation of $^1O_2$ by PMS. Although TBA could also be directly oxidized by PMS and thus consume part of it (explaining the inhibitory effect in the first 60 min), the intermediates (or reactive species) produced by TBA and PMS may have a synergistic effect with $^1O_2$.

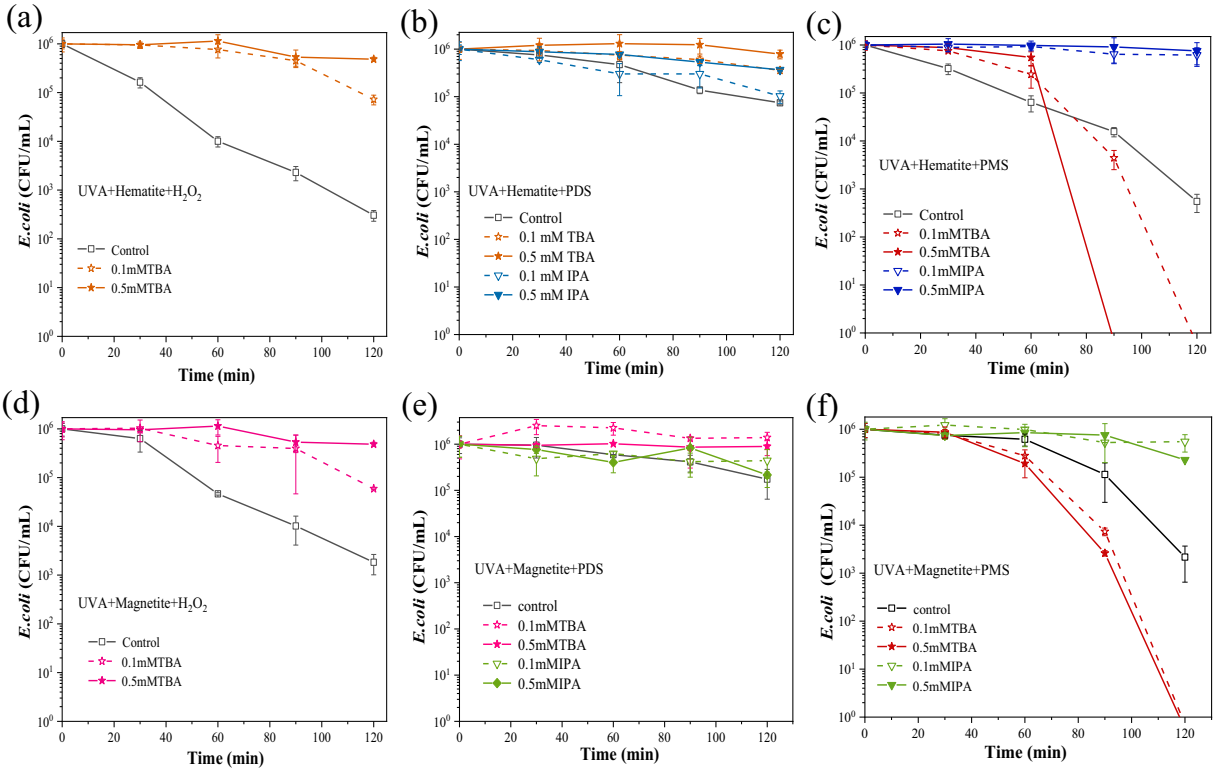

Fig. 6. Quenching experiments in different combined systems. Experimental conditions: [iron oxides] = 1 mg/L, [oxidants] = 10 mg/L, [pH] = 7.5. Experiments were performed in triplicate (the standard error was found to be of ~5 %).

3.7. Pathways to inactivation: an integrated proposal for the disinfection of E. coli by the UVA/iron oxide/oxidant system

Based on the EPR/scavenging results, material characteristics, and relevant reports, it can be concluded that the integrated inactivation mechanisms of the proposed systems are shown in Fig. 7. The main inactivation pathways are as follows:

(1) Iron oxide semiconductors produce electrons and holes when exposed to ultraviolet (UV) light. As electron acceptors, oxidants would react with the photogenerated electrons and form the corresponding reactive species ($SO_4^{\bullet-}$ and ·OH, which mainly occurred in the PDS and H_2O_2 groups) (pathway 1). In addition, holes in iron oxides can directly attack bacteria, causing bacterial death (pathway 2).

(2) At pH 7.5, although iron oxides easily agglomerate and exist in insoluble forms, oxidants can induce the formation of surface complexes with iron oxides. The LMCT process would occur and induce the formation of reactive species for bacterial inactivation (pathway 3). The formed iron-oxidant complexes also provide the possibility of a series of reactions between the three oxidants and surface iron in different valence states (pathway 4). For the PMS-involved systems, $^1O_2$ was the main reactive species and was mainly derived from $SO_5^{\bullet-}$ (pathway 5), the dismutation of PMS could also induce the generation of $^1O_2$ (pathway 6).

(3) Iron oxide particles can attach to the bacterial wall, and LMCT occurs in the iron-bacterial cell wall complex under light irradiation; during this process, the cell wall acts as an electron donor, and the integrity of the cell is impaired (pathway 7). The generated Fe^{2+} enhances the intracellular photo-Fenton process owing to Fe^{2+} diffusion, and in the case of H_2O_2, it is transferred inside the cell (pathway 8).

4. Conclusions

In this study, the inactivation behavior of low dosage hematite and magnetite-mediated three oxidants (H_2O_2, PDS, and PMS)-involved photo-Fenton-like systems under low-intensity UVA irradiation was systematically investigated and compared. The results are summarized as follows:

(1) Over pH range of 5–8, iron oxides-mediate PMS-involved photo-Fenton-like system could be considered as a substitute to the photo-Fenton one, and the outcome of hematite-mediated systems was always better than those based on magnetite. Additionally, hematite alone as a photocatalyst could also achieve good inactivation performance, which is meaningful because the avoidance of oxidants could reduce the cost of the treatment and avoid secondary pollution.

(2) The introduction of HA to the iron oxides severely inhibited the inactivation efficiency of H_2O_2-involved system, and slightly inhibited UVA/hematite/PDS and UVA/magnetite/PMS systems. However, a stimulating effect occurred in UVA/hematite/PMS system (greater promotion) and UVA/magnetite/PDS system (mild promotion). The inhibitory and promoting effects were closely related to the reactive species generated in each combined system, and the reactivity of iron-organo-complexes with different oxidants.

(3) Regarding the mechanism of constructed heterogeneous photo-Fenton-like systems, in addition to the mechanism of iron-oxide semiconductors photocatalysis and UVA-activated oxidants, the iron-complexes (iron-oxidant complexes and iron-bacteria complexes) mediated-LMCT processes also made a non-negligible contribution to bacteria inactivation.

(4) In the H_2O_2 and PDS systems, ·OH was the main radical responsible for the inactivation of *E. coli*, whereas $^1O_2$ was the

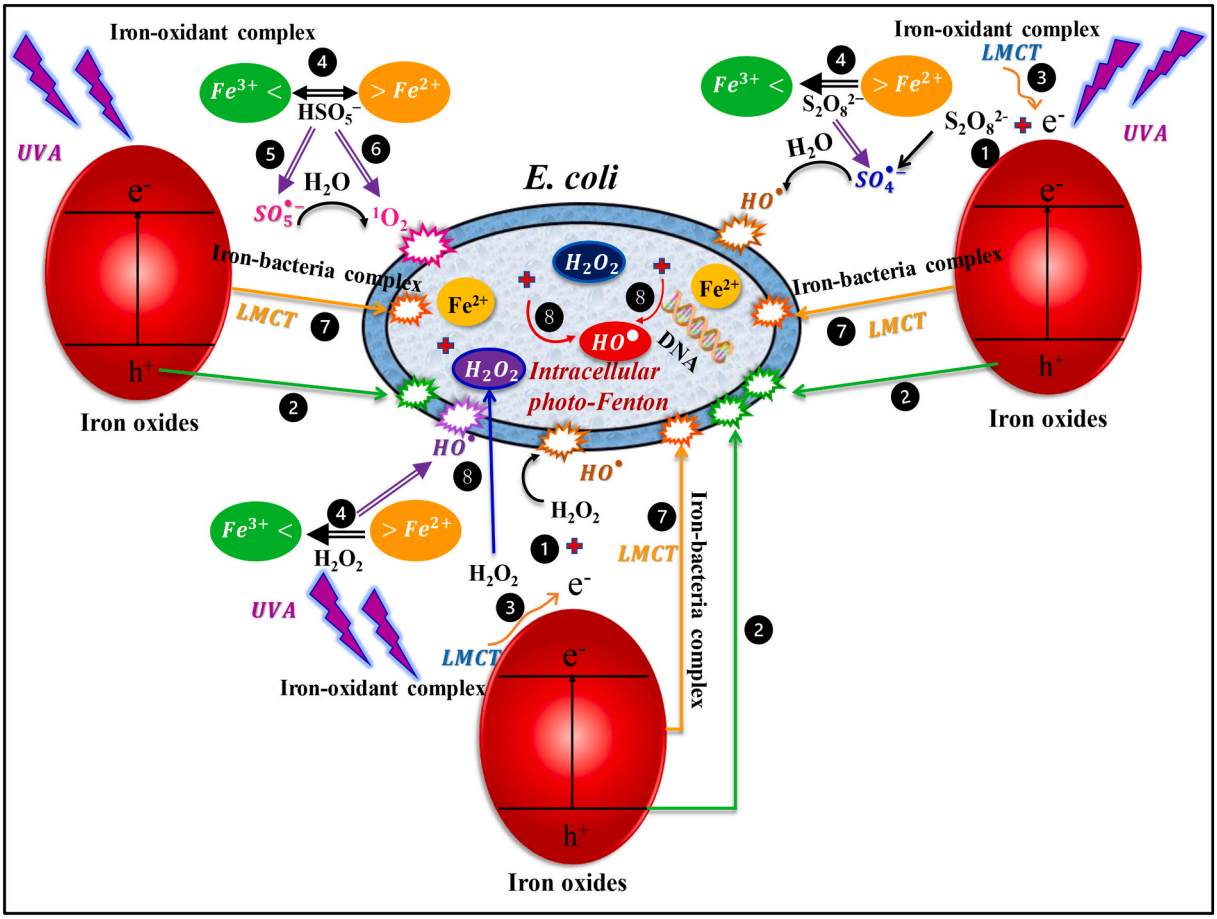

Fig. 7. Integrated mechanistic proposition for the inactivation of *E. coli* in the constructed photo-Fenton-like system.

predominant reactive species in the PMS systems.

In conclusion, this work provides some insights into the photo-Fenton-like process mediated by iron oxides, this process uses small concentration of reagents and sunlight which means that it could eventually be scaled up to treat a certain amount of water, or better yet wastewater in open reactors.

CRediT authorship contribution statement

Jialin Jia: Writing – original draft, Methodology, Investigation, Formal analysis. **Marco Minella:** Writing – review & editing. **Isabel del Castillo González:** Formal analysis. **Aurelio Hernández Lehmann:** Formal analysis. **Dong Li:** Methodology, Formal analysis. **Nuno P.F. Gonçalves:** Writing – review & editing, Methodology. **Alessandra Bianco Prevot:** Writing – review & editing. **Tao Lin:** Writing – review & editing. **Stefanos Giannakis:** Writing – review & editing, Validation, Conceptualization.

Declaration of competing interest

The authors declare that they have no known competing financial interests or personal relationships that could have influenced the work reported in this study.

Data availability

No data was used for the research described in the article.

Acknowledgments

This work was supported by funds from the National Key P&D Program of China (2022YFC3203702), the Science and Technology Development Plans of the Ministry of Housing and Urban-Rural Development (2021-*K*-131), and the Six Talent Peaks Project in Jiangsu Province (JNHB-004). China Scholarship Council (202006120369), Jiangsu Funding Program for Excellent Postdoctoral Talent (2023ZB646), and Hohai University full-time postdoctoral research fund (2016-423278). National Natural Science Foundation of China for Youth (22306101). Stefanos Giannakis would like to acknowledge the REDDIS project, "Procesos reductivos como el Talón de Aquiles bacteriano en la desinfección de aguas residuales y en aguas naturales", which received funding from the Agencia Estatal de Investigación (Spain), "Proyectos Consolidación Investigadora 2022" (CNS2022-135728), as well as the DETRAS Project, "Desinfección-Descontaminación de Efluentes Contra la Transmisión de la Resistencia en Antibióticos" (APOYO-JOVENES-21-UXUKHL-88-WQWWQF), funded by the Comunidad de Madrid through the call "Research Grants for Young Investigators from Universidad Politécnica de Madrid". Nuno Gonçalves acknowledges funding from the European Union's Horizon Europe Research and Innovation Programme under the Marie Skłodowska-Curie Actions PF grant agreement No 101065059. Marco Minella and Alessandra Bianco Prevot acknowledge support from the Project CH4.0 under the MUR program "Dipartimenti di Eccellenza 2023-2027" (CUP: D13C22003520001).

Appendix A. Supplementary data

Supplementary data to this article can be found online at https://doi.org/10.1016/j.scitotenv.2024.172740.

References

Andreozzi, R., Caprio, V., R., 2003. Marotta Iron (III) (hydr)oxide-mediated photooxidation of 2-aminophenol in aqueous solution: a kinetic study. Water Res. 37, 3682–3688.

Anipsitakis, G.P., Tufano, T.P., Dionysiou, D.D., 2008. Chemical and microbial decontamination of pool water using activated potassium peroxymonosulfate. Water Res. 42, 2899–2910.

Aparicio, F., Escalada, J.P., Gerónimo, E.D., Aparicio, V.C., Einschlag, F.S.G., Magnacca, G., Carlos, L., Mártire, D.O., 2019. Carbamazepine degradation mediated by light in the presence of humic substances-coated magnetite nanoparticles. Nanomaterials 9, 1–12.

Asadishad, B., Ghoshal, S., Tufenkji, N., 2013. Short-term inactivation rates of selected Gram-positive and Gram-negative bacteria attached to metal oxide mineral surfaces: role of solution and surface chemistry. Environ. Sci. Technol. 47, 5729–5737.

Berruti, I., López, M.I.P., Oller, I., Laurenti, E., Minella, M., P., 2023. Calza the reactivity of peroxymonosulfate towards sulfamethoxazole. Catal. Today 413-415, 113975.

Brame, J., Li, Q., P.J.J., 2011. Alvarez nanotechnology-enabled water treatment and reuse: emerging opportunities and challenges for developing countries. Trends Food Sci. Technol. 22, 618–624.

Buxton, G.V., Bydder, M., Salmon, G. Arthur, 1999. The reactivity of chlorine atoms in aqueous solution Part II. The equilibrium $SO_4^{\cdot-} + Cl\text{-}Cl^{Nsbd} + SO_4^{2-}$. Phys. Chem. Chem. Phys. 1 (1), 269–273.

Carlos, L., Mártire, D.O., Gonzalez, M.C., Gomis, J., Bernabeu, A., Amat, A.M., Arques, A., 2012. Photochemical fate of a mixture of emerging pollutants in the presence of humic substances. Water Res. 46, 4732–4740.

Chen, J., Chu, K., Sun, S.Q., Chen, H., Song, B.H., Wang, J.H., Liu, Z.D., Zhu, L., 2023. Synthesis of magnetic core-shell Fe_3O_4-Mn_3O_4 composite for degradation of sulfadiazine via peroxymonosulfate activation: characterization, mechanism and toxicity analysis. J. Environ. Eng. 11, 109230.

Colón, D., Weber, E.J., Anderson, J.L., 2008. Effect of natural organic matter on the reduction of nitroaromatics by Fe (II) species. Environ. Sci. Technol. 42 (17), 6538–6543.

Dong, C.C., Bao, Y., Sheng, T., Yi, Q.Y., Zhu, Q.H., Shen, B., Xing, M.Y., Lo, I.M.C., Zhang, J.L., 2021. Singlet oxygen triggered by robust bimetallic MoFe/TiO_2 nanospheres of highly efficacy in solar-light-driven peroxymonosulfate activation for organic pollutants removal. Appl. Catal. B Environ. 286, 119930.

Elias, H., Gotz, U., Wannowius, K.J., 1994. Kinetics and mechanism of the oxidation of sulfur (Iv) by peroxomonosulfuric acid anion. Atmos. Environ. 28, 439–448.

Emin, S., De Respinis, M., Mavrïc, T., Dam, B., Valant, M., W.A., 2016. Smith Photoelectrochemical water splitting with porous α-Fe_2O_3 thin films prepared from Fe/Fe-oxide nanoparticles. Appl. Catal. A. 523, 130–138.

Feng, J.R., Zhang, Y., 2023. Ascorbic acid enhanced $CuFe_2O_4$-catalyzed heterogeneous photo-Fenton-like degradation of phenol. J. Environ. Chem. Eng. 11, 111009.

Gaidhane, M., Taikar, D., Gaidhane, P., Nagde, K., 2023. Nanocrystalline α-Fe_2O_3: a superparamagnetic material for w-LED application and waste water treatment. Chemical Data Collections 47, 101083.

García-Ballesteros, S., Grimalt, J., Berto, S., Minella, M., Laurenti, E., Vicente, R., López-Pérez, M.F., Amat, A.M., Prevot, A.B., Arques, A., 2018. ACS Omega 3, 13073–13080.

García-Fernández, I., Polo-López, M.I., Oller, I., Fernández-Ibáñez, P., 2012. Bacteria and fungi inactivation using Fe^{3+}/sunlight, H_2O_2/sunlight and near neutral photo-Fenton: a comparative study. Appl. Catal. B Environ. 121–122, 20–29.

Giannakis, S., Lin, K.Y.A., Ghanbari, F., 2021. A review of the recent advances on the treatment of industrial wastewaters by Sulfate Radical-based Advanced Oxidation Processes (SR-AOPs). Chem. Eng. J. 406, 127083.

Gonçalves, N.P.F., Minella, M., Fabbri, D., Calza, P., Malitesta, C., Mazzotta, E., Prevota, A.B., 2020. Humic acid coated magnetic particles as highly efficient heterogeneous photo-Fenton materials for wastewater treatments. Chem. Eng. J. 390, 124619.

Gonçalves, N.P.F., Minella, M., Mailhot, G., Brigante, M., Prevot, A.B., 2021. Photo-activation of persulfate and hydrogen peroxide by humic acid coated magnetic particles for Bisphenol A degradation. Catal. Today 361, 43–49.

Gualda-Alonso, E., Pichel, N., Soriano-Molina, P., Olivares-Ligero, E., Cadena-Aponte, F. X., Agüera, A., Sánchez Pérez, J.A., Casas López, J.L., 2023. Continuous solar photo-Fenton for wastewater reclamation in operational environment at demonstration scale. J. Hazard Mater. 459, 132101.

Hao, C., Shen, Y.R., Wang, Z.Y., Wang, X.H., Feng, F., Ge, C.W., Zhao, Y.T., Wang, K., 2015. Preparation and characterization of Fe_2O_3 nanoparticles by solid-phase method and its hydrogen peroxide sensing prop. ACS Sustain. Chem. Eng. 4 (3), 1069–1077.

Hasan, N., Kim, S., Kim, M.S., Thao Nguyen, N.T., Lee, C., Kim, J., 2020. Visible light-induced activation of peroxymonosulfate in the presence of ferric ions for the degradation of organic pollutants. Sep. Purif. Technol. 240, 116620.

Huang, H.H., Lu, M.C., Chen, J.N., 2001. Catalytic decomposition of hydrogen peroxide and 2-chlorophenol with iron oxides. Water Res. 35, 2291–2299.

Jia, J.L., Liu, D.M., Tian, J.Y., Wang, W., Ni, J.X., Wang, X., 2020. Visible-light-excited humic acid for peroxymonosulfate activation to degrade bisphenol A. Chem. Eng. J. 400, 125853.

Jiang, L.L., Zhang, Y., Zhou, M.H., Liang, L., Li, K.R., 2018. Oxidation of Rhodamine B by persulfate activated with porous carbon aerogel through a non-radical mechanism. J. Hazard. Mater. 358, 53–61.

Jiménez, I.O., Giannakis, S., Grandjean, D., Grandjean, F., Grunauer, G., López, J.L.C., Pérez, J.A.S., Pulgarin, C., 2020. Unfolding the action mode of light and homogeneous *vs.* heterogeneous photo-Fenton in bacteria disinfection and concurrent elimination of micropollutants in urban wastewater, mediated by iron oxides in raceway pond reactors. Appl. Catal. B Environ. 263, 118158.

Kolhe, N.D., Walekar, L.S., Kadam, A.N., Chopade, A.S., Lee, S.W., Mhamane, D.S., Shringare, S.N., Lawand, A.S., Lawand, G.S., Misra, M., Mali, M.G., 2023. MOF derived *in-situ* construction of core-shell Z-scheme $BiVO_4$@α-Fe_2O_3-CF nanocomposites for efficient photocatalytic treatment of organic pollutants under visible light. J. Clean. Prod. 420, 138179.

Li, X.N., Huang, X., Xi, S.B., Miao, S., Ding, J., Cai, W.Z., Liu, S., Yang, X.L., Yang, H.B., Gao, J.J., Wang, J.H., Huang, Y.Q., Zhang, T., Liu, B., 2018. Single cobalt atoms

anchored on porous N-doped graphene with dual reaction sites for efficient Fenton-like catalysis. J. Am. Chem. Soc. 140 (39), 12469–12475.
Li, D.H., Zhang, S.X., Li, S.N., Tang, J.C., Hua, T., Li, F.X., 2023a. Mechanism of the application of single-atom catalyst-activated PMS/PDS to the degradation of organic pollutants in water environment: a review. J. Clean. Prod. 397, 136468.
Li, Y.H., Wang, C.C., Wang, F., Liu, W., Chen, L., Zhao, C., Fu, H.F., Wang, P., Duan, X.G., 2023b. Nearly zero peroxydisulfate consumption for persistent aqueous organic pollutants degradation via non-radical processes supported by in-situ sulfate radical regeneration in defective MIL-88B(Fe). Appl. Catal. B Environ. 331, 122699.
López-Vinent, N., Cruz-Alcalde, A., Giménez, J., Esplugas, S., 2021. Mixtures of chelating agents to enhance photo-Fenton process at natural pH: influence of wastewater matrix on micropollutant removal and bacterial inactivation. Sci. Total Environ. 786, 147416.
Lopez-Vinent, N., Cruz-Alcalde, A., Moussavi, G., Gonzalez, I.C., Lehmann, A.H., Gimenez, J., Giannakis, S., 2022. Improving ferrate disinfection and decontamination performance at neutral pH by activating peroxymonosulfate under solar light. Chem. Eng. J. 450, 137904.
Machreki, M., Tyuliev, G., Zigon, D., Guo, Q., Chouki, T., Sobrido, A.B.J., Dimitrov, S., Emin, S., 2024. Photoelectrochemical activation of peroxymonosulfate using Sn-doped α-Fe_2O_3 thin film for degradation of anti-inflammatory pharmaceutical drug. J. Photoch. Photobio. A. 446, 115126.
Maji, S.K., Mukherjee, N., Mondal, A., Adhikary, B., 2012. Synthesis, characterization and photocatalytic activity of a-Fe_2O_3 nanoparticles. Polyhedron 33, 145–149.
Matta, R., Hanna, K., Chiron, S., 2007. Fenton-like oxidation of 2,4,6-trinitrotoluene using different iron minerals. Sci. Total Environ. 385, 242–251.
Mazille, F., Moncayo-Lasso, A., Spuhler, D., Serra, A., Peral, J., Benítez, N.L., Pulgarin, C., 2010. Comparative evaluation of polymer surface functionalization techniques before iron oxide deposition. Activity of the iron oxide-coated polymer films in the photo-assisted degradation of organic pollutants and inactivation of bacteria. Chem. Eng. J. 160, 176–184.
Meireles, A., Giaouris, E., Simoes, M., 2016. Alternative disinfection methods to chlorine for use in the fresh-cut industry. Food Res. Int. 82, 71–85.
Nieto-Juarez, J.I., Kohn, T., 2013. Virus removal and inactivation by iron (hydr) oxidemediated Fenton-like processes under sunlight and in the dark. Photochem. Photobiol. Sci. 12, 1596–1605.
Niu, H., Zhang, D.I., Zhang, S., Zhang, X., Meng, Z., Cai, Y., 2011. Humic acid coated Fe_3O_4 magnetic nanoparticles as highly efficient Fenton-like catalyst for complete mineralization of sulfathiazole. J. Hazard. Mater. 190 (1-3), 559–565.
Pignatello, J.J., Oliveros, E., MacKay, A., 2006. Advanced oxidation processes for organic contaminant destruction based on the Fenton reaction and related chemistry. Crit. Rev. Environ. Sci. Technol. 36, 1–84.
Pino-Sandoval, D.A., Cantú-Cárdenas, M.E., Rodríguez-González, V., Patrón Soberano, O. A., Rosas-Castor, J.M., Camilo Murillo-Sierra, J., Hernández-Ramírez, A., 2023. Solar heterogeneous photo-Fenton for complete inactivation of *Escherichia coli* and *Salmonella typhimurium* in secondary-treated wastewater effluent. Chemosphere 342, 140132.
Rodríguez-Chueca, J., Giannakis, S., Marjanovic, M., Kohantorabi, M., Reza Gholami, M., Grandjean, D., de Alencastro, L.F., Pulgarín, C., 2019. Solar assisted bacterial disinfection and removal of contaminants of emerging concern by Fe^{2+}-activated HSO_5^- vs. $S_2O_8^{2-}$ in drinking water. Appl. Catal. B Environ. 248, 62–72.
Rose, A.L., Waite, T.D., 2003. Effect of dissolved natural organic matter on the kinetics of ferrous iron oxygenation in seawater. Environ. Sci. Technol. 37, 4877.
Ruales-Lonfat, C., Benítez, N., Sienkiewicz, A., Pulgarín, C., 2014. Deleterious effect of homogeneous and heterogeneous near-neutral photo-Fenton system on Escherichia coli. Comparison with photo-catalytic action of TiO_2 during cell envelope disruption. Appl. Catal. B Environ. 160–161, 286–297.
Ruales-Lonfat, C., Barona, J.F., Sienkiewicz, A., Bensimon, M., Vélez-Colmenares, J., Benítez, N., C., 2015. Pulgarín Iron oxides semiconductors are efficient for solar water disinfection: a comparison with photo-Fenton processes at neutral pH. Appl. Catal. B Environ. 166–167, 497–508.
Spuhler, D., Andrés Rengifo-Herrera, J., Pulgarin, C., 2010. The effect of Fe^{2+}, Fe^{3+}, H_2O_2 and the photo-Fenton reagent at near neutral pH on the solar disinfection (SODIS) at low temperatures of water containing Escherichia coli K12. Appl. Catal. B Environ. 96, 126–141.
Sundaresan, K., Mohan, S., Manojkumar, M.S., Sakthisaravanan, M.V., Raja, M. Shkir, Ali, H.E., 2023. Magneto recyclable, green fabricated Fe_3O_4 nanorods on photo responsive of textile dye degradation and identification products by LC-MS. J. Indian Chem. Soc. 100, 10093.
Tian, N., Schmidt, L.C., Lameiro, M.J.A., Polo-López, M.I., Marín, M.L., Boscá, F., González, I.C., Lehmann, A.H., Giannakis, S., 2024. Why is HSO_5^- so effective against bacteria? Insights into the mechanisms of *Escherichia coli* disinfection by unactivated peroxymonosulfate. Water Res. 254, 121441.
Vikesland, P.J., Heathcock, A.M., Rebodos, R.L., Makus, K.E., 2007. Particle size and aggregation effects on magnetite reactivity towards carbon tetrachloride. Environ. Sci. Technol. 41, 5277–5283.
Walling, C., Goosen, A., 1973. Mechanism of the ferric ion catalyzed decomposition of hydrogen peroxide, effect of organic substrates. J. Am. Chem. Soc. 95, 2987–2991.
Wang, H.Z., Guo, W.Q., Liu, B.H., Wang, Q.L., Wang, H.C., Zhao, Q., Si, Q.S., Sseguya, F., Ren, N.Q., 2019. Edge-nitrogenated biochar for efficient peroxydisulfate activation: an electron transfer mechanism. Water Res. 160, 405–414.
Wu, L., Jiang, G.Y., Wang, X.N., Wang, Y., Zhou, Y.R., Wu, Z.X., 2022. Amorphous iron oxides anchored on BiOCl nanoplates as robust catalysts for high-performance photo-Fenton oxidation. J. Colloid Interface Sci. 622, 62–74.
Xu, P., Zeng, G.M., Huang, D.L., Feng, C.L., Hu, S., Zhao, M.H., Lai, C., Wei, Z., Huang, C., Xie, G.X., Liu, Z.F., 2012. Use of iron oxide nanomaterials in wastewater treatment: a review. Sci. Total Environ. 424, 1–10.
Yamashita, T., Hayes, P., 2008. Analysis of XPS spectra of Fe^{2+} and Fe^{3+} ions in oxide materials. Appl. Surf. Sci. 254, 2441–2449.
Yang, W.L., Deng, Z.J., Liu, L.B., Zhou, K.C., S, P.E., Meng, L.C., Ma, L., Wei, Q.P., 2023. Co-generation of hydroxyl and sulfate radicals via homogeneous and heterogeneous bi-catalysis with the EO-PS-EF tri-coupling system for efficient removal of refractory organic pollutants. Water Res. 243, 120312.
Zhang, J., Song, F., Li, T., Xie, K., Yao, H., Xing, B., Li, Z., Bai, Y., 2020. Simulated photodegradation of dissolved organic matter in lakes revealed by three-dimensional excitation-emission matrix with regional integration and parallel factor analysis. J. Environ. Sci. 90, 310–320.
Zhou, X., Yang, Z.Z., Chen, Y., Feng, H.P., Yu, J.F., Tang, J.L., Ren, X.Y., Tang, J., Wang, J.J., Tang, L., 2022. Single-atom Ru loaded on layered double hydroxide catalyzes peroxymonosulfate for effective *E. coli* inactivation via a non-radical pathway: efficiency and mechanism. J. Hazard. Mater. 440, 129720.